Monodispersed InP Quantum Dots Prepared by Colloidal Chemistry in a Noncoordinating Solvent

Derrick W. Lucey, David J. MacRae, Madalina Furis, Yudhisthira Sahoo, Alexander N. Cartwright, and Paras N. Prasad*

Departments of Chemistry, Physics, and Electrical Engineering, Institute for Lasers, Photonics and Biophotonics, State University of New York, Buffalo, New York 14260

Received January 18, 2005. Revised Manuscript Received March 4, 2005

III−V semiconductor quantum dots are of considerable interest as their applications cover a broad spectrum, from optoelectronic to biomedical technology. For them to be of practical value, there is a need for a method that provides rapid and scalable production of highly monodispersed nanoparticles. This paper reports an efficient and rapid method of producing highly monodispersed InP quantum dots using a novel precursor-based colloidal synthesis in a noncoordinating solvent. The method also allows judicious control over the size of the quantum dots and can also be extended to produce other III−V quantum dots. In this paper, the synthesis and characterization of highly monodispersed InP quantum dots from newly prepared indium(III) carboxylate complexes in octadecene are detailed. When using indium(III) carboxylate as the indium precursor, no surfactant or coordinating solvents are required to prepare high-quality InP quantum dots in octadecene. The in situ formation of a surfactant upon injection of the phosphine precursor [$P(SiMe_3)_3$] helps control the growth of the resulting quantum dots. Structural and optical studies (continuous wave and time-resolved) have been performed on the as-prepared InP quantum dots. In addition, time-resolved photoluminescence has been conducted on etched InP quantum dots. The effects of the carboxylate chain length in indium(III) carboxylate and injection temperature on the growth and properties of quantum dots have been studied.

Introduction

The synthesis of III−V semiconductor nanocrystals has been an area of intense research over the past 20 years. Since Wells et al.[1] first demonstrated the dehalosilylation reaction in the synthesis of InAs and GaAs, many other groups have spent considerable time and effort on solution phase synthesis of III−V semiconductor nanoparticles.[2−27] The principal interest in semiconductor nanoparticles [or quantum dots (QDs)] lies in their optical properties which are dramatically affected by quantum confinement. Since QD physical dimensions are comparable to the carrier de Broglie wave function in semiconductors, energy states of the electrons and holes are quantized.[28] As a result, the emission efficiencies of semiconductor QDs are substantially higher than those of their bulk counterparts, and most importantly, the emission wavelength varies as a function of dot size.[29] These properties

* To whom correspondence should be addressed. E-mail: pnprasad@buffalo.edu.

(1) Wells, R. L.; Pitt, C. G.; McPhail, A. T.; Pardy, A. P.; Shafieezad, S.; Hallock, R. B. *Chem. Mater.* **1989**, *1*, 4−6.
(2) Guzelian, A. A.; Katari, J. E. B.; Kadavanich, A. V.; Banin, U.; Hamad, K.; Juban, E.; Alivisatos, A. P.; Wolters, R. H.; Arnold, C. C.; Heath, J. R. *J. Phys. Chem.* **1996**, *100*, 7212−7219.
(3) Micic, O. I.; Curtic, C. J.; Jones, K. M.; Sprague, J. R.; Nozik, A. J. *J. Phys. Chem.* **1994**, *98*, 4966−4969.
(4) Micic, O. I.; Sprague, J. R.; Curtic, C. J.; Jones, K. M.; Machol, J. L.; Nozik, A. J.; Giessen, H.; Fluegel, B.; Mohs, G.; Peyghambarian, N. *J. Phys. Chem.* **1995**, *99*, 7754−7759.
(5) Talapin, D. V.; Rogach, A. L.; Mekis, I.; Haubold, S.; Kornowski, A.; Haase, M.; Weller, H. *Colloids Surf., A* **2002**, *202*, 145−154.
(6) Micic, O. I.; Ahrenkiel, S. P.; Nozik, A. J. *Appl. Phys. Lett.* **2001**, *78*, 4022−4024.
(7) Langof, L.; Ehrenfreund, E.; Lifshitz, E.; Micic, O. I.; Nozik, A. J. *J. Phys. Chem. B* **2002**, *106*, 1606−1612.
(8) Micic, O. I.; Sprague, J.; Lu, Z.; Nozik, A. J. *Appl. Phys. Lett.* **1996**, *68*, 3150−3152.
(9) Micic, O. I.; Cheong, H. M.; Fu, H.; Zunger, A.; Sprague, J. R.; Mascarenhas, A.; Nozik, A. J. *J. Phys. Chem. B* **1997**, *101*, 4904−4912.
(10) Fu, H.; Zunger, A. *Phys. Rev. B* **1997**, *56*, 1496−1508.
(11) Bertram, D.; Micic, O. I.; Nozik, A. J. *Phys. Rev.* **1998**, *57*, R4265−R4268.
(12) Talapin, D. V.; Gaponik, N.; Borchert, H.; Rogach, A. L.; Haase, M.; Weller, H. *J. Phys. Chem. B* **2002**, *106*, 12659−12663.
(13) Micic, O. I.; Nozik, A. J.; Lifshitz, E.; Rajh, T.; Poluektov, O. G.; Thurnauer, M. C. *J. Phys. Chem. B* **2002**, *106*, 4390−4395.
(14) Furis, M.; MacRae, D. J.; Lucey, D. W.; Sahoo, Y.; Cartwright, A. N.; Prasad, P. N. *Mater. Res. Soc. Symp. Proc.* **2003**, *N3.35*, 54490.
(15) Douglas, T.; Theopold, K. H. *Inorg. Chem.* **1991**, *30*, 594−596.
(16) Trentler, T. J.; Hickman, K. M.; Goel, S. C.; Viano, A. M.; Gibbons, P. C.; Buhro, W. E. *Science* **1995**, *270*, 1791−1794.
(17) Trentler, T. J.; Goel, S. C.; Hickman, K. M.; Viano, A. M.; Chiang, M. Y.; Beatty, A. M.; Gibbons, P. C.; Buhro, W. E. *J. Am. Chem. Soc.* **1997**, *119*, 2172−2181.
(18) Yu, H.; Li, J.; Loomis, R. A.; Wang, L.-W.; Buhro, W. E. *Nat. Mater.* **2003**, *2*, 517−520.
(19) Ahrenkiel, S. P.; Micic, O. I.; Miedaner, A.; Curtis, C. J.; Nedeljkovic, J. M.; Nozik, A. J. *Nano Lett.* **2003**, *3*, 833−837.
(20) Nedeljkovic, J. M.; Micic, O. I.; Ahrenkiel, S. P.; Miedaner, A.; Nozik, A. J. *J. Am. Chem. Soc.* **2004**, *126*, 2632−2639.
(21) Green, M.; O'Brien, P. *Chem. Commun.* **1998**, 2459−2460.
(22) Yan, P.; Xie, Y.; Wang, W.; Liu, F.; Qian, Y. *J. Mater. Chem.* **1999**, *9*, 1831−1833.
(23) Li, B.; Xie, Y.; Huang, J.; Liu, Y.; Qian, Y. *Ultrason. Sonochem.* **2001**, *8*, 331−334.
(24) Wei, S.; Lu, J.; Zeng, L.; Yu, W.; Qian, Y. *Chem. Lett.* **2002**, 1034−1035.
(25) Gao, S.; Lu, J.; Chen, N.; Zhao, Y.; Xie, Y. *Chem. Commun.* **2002**, 3064−3065.
(26) Wei, S.; Lu, J.; Yu, W.; Qian, Y. *J. Appl. Phys.* **2004**, *95*, 3683−3688.
(27) Battaglia, D.; Peng, X. *Nano Lett.* **2002**, *2*, 1027−1030.
(28) Prasad, P. N. *Nanophotonics*; John Whiley & Sons: New York, 2004.
(29) Alivisatos, A. P. *Science* **1996**, *271* (5251), 933−937.

10.1021/cm050110a CCC: $30.25
Published on Web 06/15/2005

make colloidal dots, readily dispersable in a host medium, very attractive for optical device applications such as hybrid light-emitting diodes,[30] photorefractive devices,[31] and potential laser development.[32] Furthermore, the "dark" (optically forbidden) character of the lowest exciton state[33] and the long carrier lifetimes measured[34] in colloidal dots are characteristics which make QDs good candidates for spintronics and quantum computing applications.

The main advantages offered by III−V semiconductor nanocrystals (as opposed to the II−VI QDs which are already commercially available) lie in the robustness of the covalent bond in III−V semiconductors versus the ionic bond in the II−VI semiconductors and in the reduced toxicity of compounds such as InP. This makes III−V quantum dots (e.g., InP) a potentially better candidate than II−VI quantum dots (e.g., CdSe) for biological applications such as bioimaging or photodynamic therapy.

This work reports the synthesis of high-purity indium(III) carboxylate precursors, where the carboxylate is myristate, stearate, and laurate, via direct elimination of cyclopentadiene. These high-purity indium(III) carboxylate precursors have enabled us to report the first nanoparticle preparation that yields size selective QDs without the addition of coordinating solvents, ligands, or surfactants. Synthesis and characterization of $InP_{(QDs)}$ utilizing this new synthetic approach are detailed here. Effects such as temperature and carboxylate chain length on InP quantum dots [$InP_{(QDs)}$] are explored and discussed. All $InP_{(QDs)}$ reactions were assessed as a function of growth time by absorption and fluorescence spectroscopy. These spectra exhibit relatively sharp features which confirm that narrow size distributions can be obtained through the growth method described here, without the need for a post-growth size selective precipitation often used to isolate a narrow size distribution. Similar measurements, performed after the samples have undergone an HF etching process, indicate the emission efficiencies of the $InP_{(QDs)}$ are as large as 18%. The results of preliminary time-resolved photoluminescence measurements are also discussed.

Experimental Section

Synthesis. $In(C_5H_5)_3$ was prepared according to the literature method.[35] Tris(trimethylsilyl)phosphine [$P(TMS)_3$], myristic acid, stearic acid, lauric acid, and technical grade (90%) 1-octadecene tech (ODE) were purchased from Aldrich Chemical Co. All solvents were carefully dried by using conventional procedures. All compounds described in this investigation were treated as if they were sensitive to oxygen and moisture, and were manipulated either under a purified argon atmosphere in a Vacuum Atmospheres drybox or by using standard vacuum line techniques unless otherwise mentioned. The first chemical purposefully exposed to air was $InP_{(QDs)}$ upon completion of their synthesis.

Synthesis of Indium(III) Precursors. Within the glovebox, a 500 mL three-neck round-bottom flask was loaded with a 3.01:1 molar ratio of carboxylic acid to $In(C_5H_5)_3$ and a stir bar and equipped with a glass stopper, a coarse-grained sintered frit connected to a one-neck 300 mL round-bottom flask, and a high-vacuum line adapter. Then approximately 100−150 mL of dry benzene was distilled into the reaction vessel, and the reaction was started by thawing the benzene. After 4 h at room temperature, all of the volatile components were removed by flask-to-flask distillation. Then the crude product was washed three times with 75−100 mL of dry ether, followed by three washes with 75−100 mL of dry pentane. Finally, pentane was removed, and after dynamic vacuum overnight, the sample was stored in a glovebox for future use. The typical yields of the individual indium(III) carboxylates were as follows: 63.2, 58.3, and 88.53% for indium(III) laurate, indium(III) myristate, and indium(III) stearate, respectively.

Elemental Analysis. The elemental analyses reported here were conducted by Prevalere Life Sciences, Inc. (Whitesboro, NY). For all samples, only the percentages of carbon and hydrogen were analyzed. Anal. Calcd for indium(III) laurate ($C_{36}H_{69}InO_6$): C, 60.66; H, 9.76. Found: C, 60.65; H, 9.75. Anal. Calcd for indium(III) myristate ($C_{42}H_{81}InO_6$): C, 63.30; H, 10.25. Found: C, 61.96; H, 9.98. Anal. Calcd for indium(III) stearate ($C_{54}H_{105}InO_6$): C, 67.19; H, 10.96. Found: C, 66.21; H, 11.19. For comparison. Anal. Calcd for lauric acid ($C_{12}H_{24}O_2$): C, 71.95; H, 12.08. Found: C, 71.52; H, 12.50. For comparison. Anal. Calcd for myristic acid ($C_{14}H_{28}O_2$): C, 73.63; H, 12.36. Found: C, 73.78; H, 13.82. For comparison. Anal. Calcd for stearic acid ($C_{18}H_{36}O_2$): C, 76.00; H, 12.76. Found: C, 75.76; H, 12.47.

NMR Spectroscopy. The ^1H NMR spectra were recorded at 400 MHz by using a Varian XL 400 spectrophotometer. All air-sensitive samples for the NMR spectra were contained in flame-sealed NMR tubes. Chemical shifts are reported in δ (parts per million) and are referenced to tetramethylsilane (TMS) as $\delta = 0.00$ ppm and benzene as $\delta = 7.15$ ppm. All of the indium(III) carboxylates are only slightly soluble in hot benzene, so throughout the analyses of the various complexes, the reported temperatures are the temperatures at which the spectra were collected.

Indium(III) laurate: ^1H NMR (d_6-benzene, 55 °C) δ 2.59 (br, 2H), 1.78 (quintet, $J = 7.0$ Hz, 2H), 1.32 (br, 16H), 0.924 (triplet, $J = 6.2$ Hz, 3H); ^1H NMR of lauric acid (d_6-benzene, RT) δ 12.72 (br, 1H), 2.08 (triplet, $J = 7.6$ Hz, 2H), 1.47 (quintet, $J = 7.0$ Hz, 2H), 1.25−1.13 (br-m, 16H), 0.91 (triplet, $J = 6.8$ Hz, 3H).

Indium(III) myristate: ^1H NMR (d_6-benzene, 45 °C) δ 2.55 (triplet, $J = 7.20$ Hz, 2H), 1.76 (quintet, $J = 7.2$ Hz, 2H), 1.33 (br, 20H), 0.92 (triplet, $J = 6.8$ Hz, 3H); ^1H NMR of myristic acid (d_6-benzene, RT) δ 12.57 (br, 1H), 2.08 (triplet, $J = 7.4$ Hz, 2H), 1.47 (quintet, $J = 7.2$ Hz, 2H), 1.29−1.13 (br-m, 10H), 0.91 (triplet, $J = 7.0$ Hz, 3H).

Indium(III) stearate: ^1H NMR (d_6-benzene, 55 °C) δ 2.42 (br, 2H), 1.72 (br, 2H), 1.35 (br, 28H), δ 0.91 (br, 3H); ^1H NMR of stearic acid (d_6-benzene, RT) δ 12.38 (br, 1H), 2.07 (triplet, $J = 7.6$ Hz, 2H), 1.47 (quintet, $J = 6.8$ Hz, 2H), 1.33−1.14 (br-m, 28H), 0.91 (triplet, $J = 7.0$ Hz, 3H).

Synthesis of InP Nanocrystals. Within the glovebox, the reaction vessel[36] was loaded with a stir bar and the indium precursor

(30) Tessler, N.; Medvedev, V.; Kazes, M.; Kan, S. H.; Banin, U. *Science* **2002**, *295* (5559), 1506−1508.
(31) Winiarz, J. G.; Zhang, L.; Lal, M.; Friend, C. S.; Prasad, P. N. *J. Am. Chem. Soc.* **1999**, *121*, 5287−5295.
(32) Eisler, H.-J.; Sundar, V. C.; Bawendi, M. G.; Walsh, M.; Smith, H. I.; Klimov, V. *Appl. Phys. Lett.* **2002**, *80* (24), 4614−4616.
(33) Crooker, S. A.; Barrick, T.; Hollingsworth, J. A.; Klimov, V. *Appl. Phys. Lett.* **2003**, *82* (17), 2793−2795.
(34) Efros, Al. L.; Rosen, M. *Annu. Rev. Mater. Sci.* **2000**, *30*, 475−521.
(35) Beachley, O. T., Jr.; MacRae, D. J.; Kovalevsky, A. Y.; Zhang, Y.; Li, X. *Organometallics* **2002**, *21*, 4632−4640.

(36) Reaction vessel description: The reaction vessel was fabricated as a 100 mL three-neck U-bottom flask with the right and left necks being #7 Chem-Thread adaptors from chemglass and the middle neck as a 19/38 Wheaton Clear Seal female adaptor. A reflux condenser is connected to the reaction flask with the male 19/38 Wheaton Clear Seal adaptor, and the condenser top is a 24/40 ground glass adaptor. A glass thermometer holder is placed in the right #7 Chem-Thread adaptor, while a rubber septum is placed in the other #7 Chem-Thread adaptor.

(approximately 500 μmol). Also within the glovebox, approximately 250 μmol of $P(TMS)_3$ was loaded into a four-dram vial containing ~4 mL of dry ODE and capped with a rubber septa. After removal from the glovebox, the reaction vessel was placed in a 500 mL round-bottom heating mantle which was filled with sand. Then the reaction vessel was connected to a Schlenk line, and with an argon flow, 40 mL of ODE was added via a syringe. Next, with the stirrer going, the temperature was set to 100 °C and the reaction vessel was placed under vacuum for at least 1 h. Then the vessel containing a colorless optically clear solution was backfilled with Ar(g), and the temperature was set to the desired reaction temperature (250−300 °C). Once the reaction temperature was reached, the phosphine solution was rapidly injected via a 10 mL syringe. After a desired period of time, usually 1 or 10 min, an additional 40 mL of ODE was added and the temperature set to the growth temperature (200−250 °C). Throughout the reaction, the solution gradually changed color from clear and colorless to transparent yellow-orange, then transparent orange, then transparent light red, then transparent bright red, then transparent dark red, and sometimes a dark brown almost black color. The rate and extent of color change depended on the reaction temperature and time. Aliquots of the reaction mixture (0.5 mL in approximately 5 mL of chloroform or hexanes) were taken at various times (typically 1, 2.5, 5, 10, 15, 30, and 45 min and 1, 1.5, and 2 h) to follow the growth process. Most reactions were stopped after 2 h by removing the mixtures from the heat source and allowing gradual cooling to room temperature. For structural characterization, the final products of these reactions were isolated by the addition of a 4−5-fold excess of acetone to the reaction volume of ODE. Centrifugation of this mixture at 11 000 rpm for 20 min at 20 °C produced the crude product. Later it was discovered that dilution of the crude reaction product after the initial precipitation in chloroform, followed by precipitation with acetone, led to precipitation of two different species: the $InP_{(QDs)}$ which are more dense than the solvent and another solid that was less dense than the solvent. Repeated washing and removal of the precipitate on top leads to the isolation of purer $InP_{(QDs)}$.

Synthesis of InP Nanocrystals for Temperature Study and Carboxylate Chain Length Study. Within the glovebox, the reaction vessel was loaded with a stir bar and the indium(III) carboxylate precursor (approximately 250 μmol). Also within the glovebox, approximately 125 μmol of $P(TMS)_3$ was loaded into a four-dram vial containing ~4 mL of dry octadecene and capped with a rubber septum. Following the same procedures described above, the phosphine precursor was injected to start the reaction. For this temperature dependence study, the initial temperature was maintained throughout the course of the reaction. Aliquots of the reaction mixture (0.25 mL in approximately 5 mL of chloroform) were taken at various times (30 s, 1, 2.5, 5, 10, 15, 30, and 45 min, and 1, 1.5, and 2 h) to follow the growth process. The final products of these reactions were not processed further.

Characterization of $InP_{(QDs)}$. The resulting nanoparticles were characterized by UV−vis spectroscopy, photoluminescence (PL) spectroscopy, photoluminescence excitation (PLE) spectroscopy, transmission electron microscopy (TEM), energy dispersive spectroscopy (EDS), X-ray photoelectron spectroscopy (XPS), and X-ray diffraction (XRD) spectroscopy.

UV−Visible Absorbance. The absorbance spectra were measured by using a Shimadzu model 3101PC UV−vis−NIR scanning spectrophotometer or a Hewlett-Packard 8452A diode array spectrophotometer with the samples in 1 cm cuvettes.

Transmission Electron Microscopy (TEM) and Electron Diffraction (ED). Transmission electron microscopy (TEM) and electron diffraction (ED) images were obtained with a model 200 JEOL microscope at an acceleration voltage of 200 kV. Some specimens were prepared by drop casting the toluene/hexane dispersion onto an amorphous carbon-coated 300 mesh copper grid. Other specimens were prepared by drop casting chloroform dispersions onto an amorphous carbon-coated 300 or 200 mesh copper grid. Selected area electron diffraction was assessed at a camera length of 60 cm.

X-ray Photoelectron Spectroscopy (XPS). XPS studies were performed on a Physical Electronics/PHI 5300 X-ray photoelectron spectrometer with a hemispherical analyzer and a single-channel detector, operated at 300 W (15 kV and 20 mA). Mg Kα radiation (1253.6 eV) and pass energies of 89.45 eV for survey scans and 17.9 eV for high-resolution scans were used. Three samples were analyzed: indium(III) stearate, unwashed $InP_{(QDs)}$, and pyridine-washed $InP_{(QDs)}$. Indium(III) stearate, prepared as described above, was used without any further purification. The unwashed $InP/In_2O_{3(QDs)}$ were prepared as described above by treating 500 μmol of $In(stearate)_3$ in 40 mL of 240 °C ODE with 250 μmol of $P(TMS)_3$. Upon completion of the reaction, the particles were isolated by precipitating with acetone and centrifugation. The unwashed QDs were then combined into one centrifuge tube (from six tubes) by addition of chloroform followed by precipitation with methanol. After centrifugation and decantation, the QDs were placed under vacuum at RT for ~2 h and then submitted for XPS analysis. The pyridine-washed $InP_{(QDs)}$ were prepared by taking a sample of unwashed QDs and stirring it in 25−30 mL of pyridine overnight (~16 h). The QDs then were precipitated by hexane addition and centrifugation. These particles were then placed under vacuum at room temperature for ~2 h and submitted for XPS analysis. These samples were mounted by placing the powder samples directly onto sticky tape that is directly connected to the Au puck.

Energy Dispersive X-ray Spectroscopy (EDAX). EDAX was obtained with a Hitachi S-4000 field emission scanning electron microscope. The microscope operated at an electron acceleration voltage of 20 kV. The sample was cast as a thin film from the dispersion or simply used as a powder on a silicon or graphite substrate. The X-ray fluorescence beams were collected with an X-ray collection unit IXRF 500 system. Quantitative estimates of elements were made by comparing the spectra against that of a corresponding commercial standard InP crystal. The sample measured was the sample described directly above as the pyridine-washed sample.

X-ray Diffraction (XRD). X-ray diffraction spectra were recorded on a Siemens D500 spectrometer using the Cu Kα radiation. A powder of the sample, obtained by precipitating the product at the end of the reaction with acetone, was placed on a glass slide, and the scanning angle was slowly varied by rotating sample geometry. The 2θ angles that were probed were from 3° to 60° scanned at a rate of 2°/min.

Photoluminescence (PL) and Photoluminescence Excitation (PLE) Spectroscopy. Continuous wave (CW) PL and PLE spectra were acquired in the frontal geometry using a Jobin Yvon Fluorolog-3 spectrofluorometer equipped with a 400 W Xe lamp as the excitation source and a Hamamatsu R928 photomultiplier (PMT) tube as the detector. All spectra were corrected for the PMT response and/or the lamp emission spectrum. The emission of aliquots taken directly from the reaction mixtures as described in the synthesis section were collected from solutions in quartz cuvettes.

Time-Resolved Photoluminescence (TRPL) Spectroscopy. The time-resolved photoluminescence (TRPL) measurements were performed in the right angle geometry using 400 nm, 200 fs pulses with a repetition rate of 250 kHz, obtained by frequency doubling the 800 nm pulsed output of a Coherent Rega 9000 regenerative amplifier. The PL spectra were spectrally and temporally resolved

Table 1. Elemental Analysis Results for Indium(III) Carboxylates

	calcd % composition		experimental % composition	
carboxylate	carbon	hydrogen	carbon (% error)	hydrogen (% error)
laurate	60.66	9.76	60.65 (0.016)	9.75 (0.10)
myristate	63.30	10.25	61.96 (2.10)	9.98 (2.63)
stearate	67.19	10.96	66.21 (1.45)	11.19 (2.10)

using a 250IS Chromex monochromator (spectral resolution of 0.15 nm) equipped with a Hamamatsu C4334 streak camera with a typical jitter of 50 ps. All time-resolved measurements were carried out at room temperature, with the samples placed in the same 1 cm optical path quartz cuvettes used for the CW studies.

Results and Discussion

Preparation of Indium Precursors. The direct methathetical reaction between $InCl_3$ and a sodium or lithium salt of the corresponding carboxylic acid would be the least expensive pathway for the preparation of these types of precursors. In our preliminary attempts to prepare In(carboxylate)$_3$ directly utilizing a metathetical reaction (eq 1), a complex mixture of products was isolated in which halide free In(carboxylate)$_3$ could not be isolated even after Soxhlet extraction of the crude product with toluene.

$$InCl_3 + 3NaOC(O)(CH_2)_nCH_3 \xrightarrow[\text{temperature}]{\text{solvent}} In[OC(O)(CH_2)_nCH_3]_3 + 3NaCl \quad (1)$$

Since the direct metathesis reaction did not result in the isolation of pure In(carboxylate)$_3$ compounds, an elimination pathway was attempted directly from $In(C_5H_5)_3$ and the corresponding carboxylic acid (eq 2).

$$In(C_5H_5)_3 + 3HOC(O)(CH_2)_nCH_3 \xrightarrow[\text{RT}]{\text{benzene}} In[OC(O)(CH_2)_nCH_3]_3 + 3HC_5H_5 \quad (2)$$

We discovered that this elimination reaction proceeds at room temperature within 4 h to yield the corresponding indium(III) carboxylate complexes. As detailed in the Experimental Section, all of these compounds were characterized by ^{1}H NMR spectroscopy and elemental analysis. These compounds are slightly soluble in benzene at elevated temperatures. On the basis of the NMR spectroscopy results, only one indium(III) carboxylate species is present at the collection temperature with all the carboxylate ligands being equivalent. As expected, the hydrogens α to the carboxylate group are shifted downfield compared to those of the acids: 2.59, 2.55, and 2.42 ppm for indium(III) laurate, indium(III) myristate, and indium(III) stearate, respectively, versus, 2.08, 2.08, and 2.07 ppm for their corresponding acids. The β-hydrogens are also slightly shifted downfield compared to those of the acids; 1.78, 1.76, and 1.72 ppm for indium(III) laurate, indium(III) myristate, and indium(III) stearate, respectively, versus 1.47 ppm for all the corresponding acids. All the remaining hydrogens are not significantly affected by indium, relative to the corresponding acids.

The experimentally determined elemental analyses are in good agreement with the calculated values (Table 1). The largest variation is seen in the percent hydrogen of indium(III) myristate, which was off by 0.27%. This corresponds to a percent error of 2.63% which is within the 5% error limits of the analysis technique.

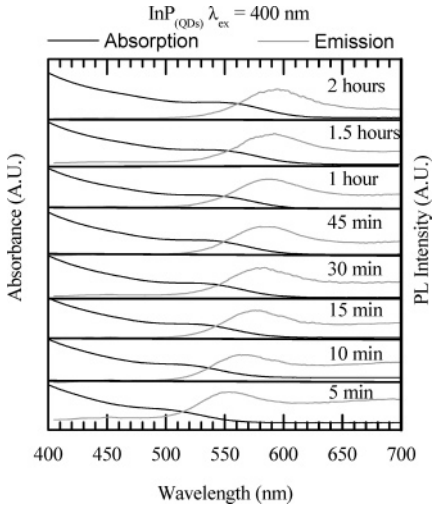

Figure 1. Typical absorption and emission spectra of $InP_{(QDs)}$.

Spectral Monitoring of in Situ Growth. With the successful synthesis of pure indium(III) carboxylate complexes, we undertook the synthesis of $InP_{(QDs)}$ as described above. This synthesis is a fast process in which nucleation is immediate after injection and the growth step can be controlled by varying the growth temperature. By taking advantage of the fast nucleation and slow growth, we prepared relatively monodispersed crops of $InP_{(QDs)}$.

Since we can control the nucleation and growth steps utilizing this fast reaction which does not utilize any surfactants, or coordinating ligands that, in some cases can, obscure the optical properties of the as-grown QDs,[37] we are able to follow the reaction progress by in situ monitoring of the absorbance, photoluminescence, and photoluminescence emission spectra. Figure 1 displays typical UV−vis and PL spectra that are obtained from aliquots taken directly from a reaction mixture. These aliquots are an example of the reaction mixture, as upon injection of the hot reaction mixture into the cool room-temperature solvents the growth should be quenched. The exact reaction parameters for the reaction used to generate Figure 1 involved injection of the phosphine precursor [P(TMS)$_3$] at 300 °C, followed by a rapid injection of 40 mL of ODE to rapidly cool the reaction mixture to the growth temperature of 245 °C. As can be seen in Figure 1A, there is a strong absorption feature after 5 min, with an absorption maximum at approximately 499 nm, which undergoes a red shift over time, at the growth temperature, to approximately 549 nm after 3 h. The full width at half-maximum (fwhm) of the absorbance feature is 68 nm after 5 min and grows to only 72 nm by the end of the reaction (3 h), indicating that there is control over the population of particles throughout the reaction.

The photoluminescence (PL) studies performed on these samples are shown in Figure 1. The photoluminescence was excited using wavelengths considerably shorter than the absorption edge of the nanocrystals (350 or 400 nm), enabling us to record the ensemble PL spectrum (or "global"

(37) Furis, M.; Sahoo, Y.; MacRae, D. J.; Manciu, F. S.; Cartwright, A. N.; Prasad, P. N. *J. Phys. Chem. B* **2003**, *107*, 11622−11625.

PL), which contains contributions from all nanocrystal sizes. For these specific reaction conditions, the PL spectrum of the "as-grown" solution contains a fairly sharp feature (60 nm fwhm after 5 min to 64 nm fwhm after reaction completion) red shifted by 46−55 nm, depending on time, with respect to the absorption edge of the nanocrystals. There is an accompanying much broader feature, on the long wavelength side of the spectrum, extending all the way into the IR region. In many cases, the broad feature dominated the spectrum. PLE spectra of the 5 min sample (Supporting Information), measured at emission wavelengths associated with the peak of the sharp PL feature (554 nm), exhibit a peak at an energy corresponding to the absorption edge of the InP nanocrystals. The sharp PL feature corresponds to the radiative recombination inside the InP nanocrystals. The origin of the broad feature (710 nm) is also related to the nanocrystals, since the PLE spectrum recorded at this wavelength is almost identical to the one associated with the sharp feature, as shown in the Supporting Information. On the basis of these observations, the sharp feature is assigned to band edge recombination in the nanocrystals and the broad feature is associated with recombination involving surface or defect-related states. It is interesting to note that the sharp feature associated with band edge recombination is already present in the PL spectrum of the reaction mixture, 5 min after the reaction has begun. As the growth progresses, the band edge:surface state emission intensity ratio increases in the favor of the former, and the entire spectrum shifts toward longer wavelengths, indicating that the nanocrystals become larger. The PL data are similar to results[2−6] reported for InP nanocrystals grown through the traditional method, with one significant difference: in all cases of the latter, a post-growth size selective precipitation must be performed on the original product to observe the sharp feature associated with band edge recombination. This is an indication that the size distributions obtained through the growth process we adopt here are comparable to the ones in previous reports, only after size-selective precipitation through the traditional methods. The emission efficiency of the as-grown nanocrystals varies from 0.5 to 2% from sample to sample. These reduced numbers can be explained by assuming insufficient surface passivation of the nanocrystals and the presence of nonradiative traps, generated by indium dangling bonds on the nanocrystal surface, as studied and discussed in detail by Fu and Zunger.[10]

Structural Characterization of Quantum Dots. A high-resolution transmission electron microscopy (HRTEM) image and a selected area electron diffraction (ED) image of a typical reaction product have been captured (Figures 2 and 3, respectively). The injection temperature for this specific reaction was 260 °C; after 10 min, ODE was added and the growth temperature was set to 200 °C. After isolation of the particles and three successive dissolutions (in $CHCl_3$), followed by precipitation with methanol, the entire sample (dissolved in ∼20 mL of $CHCl_3$) was placed in a dialysis membrane (Spectra/Por 6−8000 MWCO) and dialyzed for 24 h, with the $CHCl_3$ being changed twice. From the resulting HRTEM images (Figure 2), we can discern lattice fringes and detect crystalline $InP_{(QDs)}$. On the basis of the TEM of this sample, we were able to obtain an average size of 3.05 ± 0.32 nm (standard percent deviation of 10.5%) of particles based on a total of 85 particles.

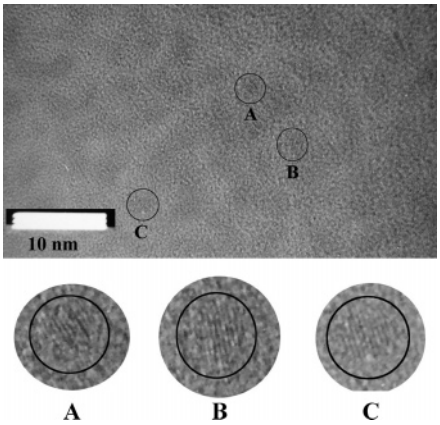

Figure 2. HRTEM image of $InP_{(QDs)}$.

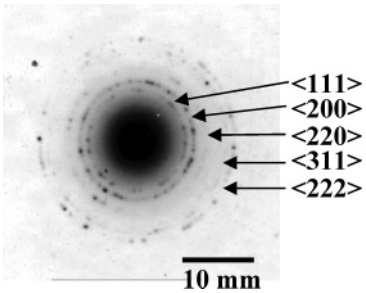

Figure 3. Selected area electron diffraction of $InP_{(QDs)}$.

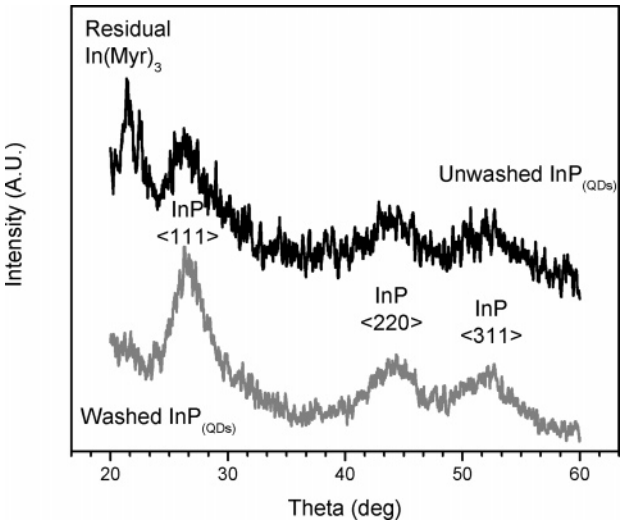

Figure 4. XRD spectra of unwashed and washed $InP_{(QDs)}$ synthesized from indium(III) myristate.

The ED patterns (Figure 3) consist of discrete rings depicting the crystalline nature of the particles. The diameters of the rings are consistent with the zinc blende phase of InP. The expected ratio of the 111, 200, 220, 311, and 222 rings is 1:1.16:1.63:1.92:2.0, which agrees well with our experimental ratio of 1:1.16:1.48:1.89:2.01.

Typical X-ray diffraction (XRD) spectra of both unwashed and washed samples are shown in Figure 4. The $InP_{(QDs)}$ used for the XRD were synthesized by injecting the phosphine at 300 °C, adding ODE after 1 min, and setting the growth temperature to 200 °C. The diffractogram agrees with the bulk zinc blende structure. The diffraction peaks for lattice

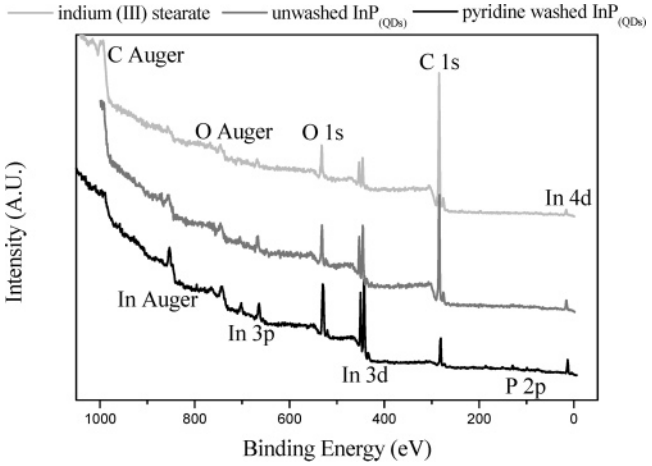

Figure 5. X-ray photoelectron survey spectra of indium(III) stearate, unwashed $InP_{(QDs)}$, and pyridine-washed $InP_{(QDs)}$.

planes ⟨111⟩, ⟨220⟩, and ⟨311⟩ are found at 2θ values of 26.6°, 44.4°, and 52.5°, respectively. The indexing gives a bulk lattice parameter of 5.9 Å. There is an extra peak at the 2θ value of 21.4° in the unwashed sample which originates from the unreacted indium myristate associated with the nanocrystals. Using the Scherrer formula $d_{\text{domain}} = (0.9\lambda/\beta \cos \theta)$, where λ is the wavelength of the X-ray and β is the full width at half-maximum (fwhm) of the diffraction peak at angle θ, the average domain size d_{domain} is found to be ∼2.86 nm. This closely agrees with the size statistics revealed by the TEM image.

X-ray photoelectron spectroscopy (XPS) was used to determine the elemental composition of indium(III) stearate, unwashed $InP_{(QDs)}$, and pyridine-washed $InP_{(QDs)}$ (Figures 5 and 6). The survey spectrum of each sample is shown in Figure 5. The survey spectra indicate the presence of indium, phosphorus, carbon, and oxygen. The presence of indium, carbon, and oxygen is easily observed in the survey spectra; however, high-resolution XPS (HR-XPS) analysis was required to observe the P 2p binding energies. Figure 6A depicts the high-resolution spectra of the P 2p region. In the two $InP_{(QDs)}$ samples, the presence of two peaks at ∼133 and ∼129 eV is obvious. Very similar binding energies have been previously reported for $InP_{(QDs)}$, prepared by the traditional TOPO method.[2] Guzelian et al.[2] reported that the P 2p peak positions of the TOPO-coated $InP_{(QDs)}$ were centered at 129.2 ± 0.2 and 133.4 ± 0.14 eV, which corresponded to phosphorus from InP and oxidized phosphine, respectively. In Figure 6B, the HR-XPS spectra of the indium binding energies are displayed. The indium core is orbit split to $3d_{5/2}$ and $3d_{3/2}$, with the $3d_{5/2}$ peak positioned at 446 eV and the $3d_{3/2}$ peak positioned at 453 eV. Guzelian et al. found that the In $3d_{5/2}$ peak varied from 444.7 to 445.6 eV.

The XPS and HR-XPS spectra show that, regardless of the sample that was analyzed, the binding energies of the indium, phosphorus, oxygen, and carbon are very similar from sample to sample, with the largest shift being 0.3 eV. When the In $3d_{5/2}$ peak binding energy of the indium precursor is compared to that of the pyridine-washed sample, there is an only 0.3 eV shift. On the basis of this study, XPS only indicates the presence of InP without providing a qualitative measure of the purity of the samples that were analyzed.

Steady State Spectroscopy of Etched Quantum Dots. To determine if the as-grown $InP_{(QDs)}$ were comparable in quality to the samples prepared utilizing the traditional synthesis approach, we treated our $InP_{(QDs)}$ with an HF etching process, very similar to those reported in the literature.[7−14] The PL spectra of three different samples are presented in Figure 7. The emission efficiencies are as high as 20% at room temperature, and the broad feature associated with the unpassivated indium dangling bond is almost entirely eliminated, confirming that its presence in the as-grown nanocrystal PL spectra is related to surface states. These efficiencies are comparable to the ones reported in the literature for $InP_{(QDs)}$.[5,8]

Time-Resolved Spectroscopy of Etched Quantum Dots. We performed time-resolved photoluminescence spectroscopy on the same samples in solution at room temperature to gain more information about carrier lifetimes and the nature of the radiative recombination. The PL intensity decay as a function of time is plotted in Figure 8 for several wavelengths across the PL profile. The decay has a multi-

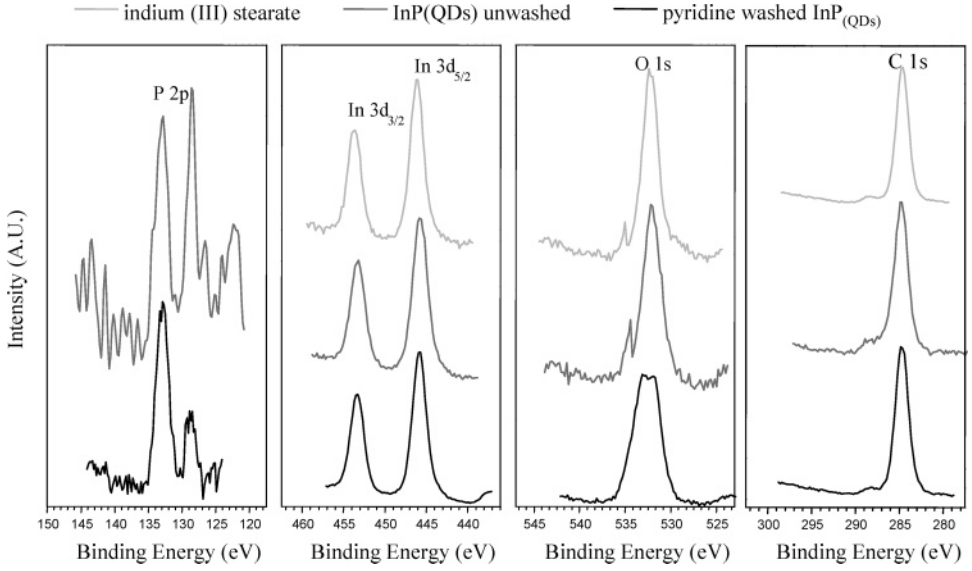

Figure 6. High-resolution X-ray photoelectron spectra of phosphorus 2p, indium 3d, oxygen 1s, and carbon 1s regions.

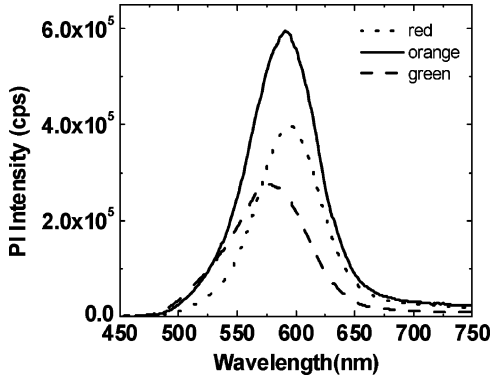

Figure 7. PL emission spectra of etched $InP_{(QDs)}$.

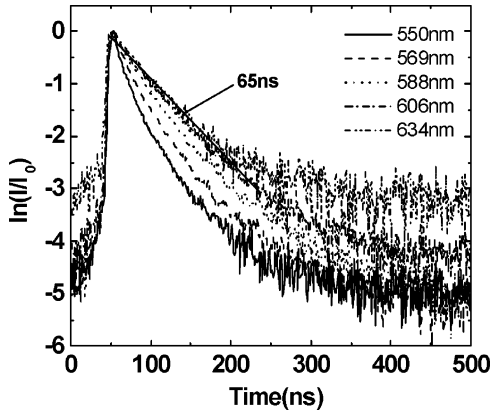

Figure 8. Time-resolved PL spectra of etched $InP_{(QDs)}$.

exponential character on the high-energy side and becomes a single exponential on the low-energy side of the PL profile. The recombination lifetimes are long (tens of nanoseconds) in comparison with typical decay times measured in bulk semiconductors. A possible explanation for the elongated lifetimes lies in the dark dipole-forbidden nature[10,38] of the lowest excitonic state. Theoretical studies predict that in semiconductor nanocrystals, the electron−hole exchange interaction lifts the 8-fold degeneracy of the band edge exciton, and the result is that the lowest-energy exciton state is an optically forbidden state. The energy splitting between the forbidden lowest-energy exciton state and the first optically allowed exciton state takes values ranging between 1 and 20 meV, depending on nanocrystal size. A dark lowest-energy exciton state would also explain the red shift of the PL with respect to the absorption edge as discussed earlier. In this framework, the absorption takes place on the optically allowed state and the excitons subsequently relax through a fast process into the long-lived, optically forbidden state where they recombine radiatively. Similar lifetimes have been measured[9] in InP nanocrystals grown through the traditional TOPO method.

The red shift we measure in the ensemble PL experiments reported here does not represent the exact allowed to forbidden (resonant) shift;[9,10] fluorescence line narrowing measurements will be performed in the future to establish the magnitude of the shift. To conclude our discussion on the results of the preliminary optical measurements, we emphasize that, despite being grown through a different approach, our InP nanocrystals exhibit optical properties which are remarkably similar to the ones measured for nanocrystals grown through a traditional method.[2−14] This study offers the possibility of establishing the influence of surfactants and/or growth parameters on the optical properties and isolating the intrinsic properties of InP nanocrystals from this influence.[36]

(38) Nirmal, M.; Norris, D. J.; Kuno, M.; Bawendi, M. G.; Efros, A. L.; Rosen, M. *Phys. Rev. Lett.* **1995**, *75*, 3728.

Table 2. Effect of Injection Temperature on the Absorption and Emission Spectra of InP(QDs) When Indium(III) Myristate Is the Precursor

time	λ_{max} (nm)	FWHM[a] (nm)	λ_{em-max}[b] (nm)	FWHM[c] (nm)	λ_{em-max}[d] (nm)	FWHM[c] (nm)
			250 °C Injection			
30 s	467	102	545	69	na[e]	na[e]
1 min	480	95	548	70	689	269
2.5 min	487	96	558	76	703	231
5 min	493	99	559	70	736	222
10 min	495	112	571	92	752	215
15 min	502	113	570	109	765	223
30 min	513	109	574	121	>785	na[e]
45 min	508	132	578	114	>785	na[e]
			260 °C Injection			
30 s	488	106	na[e]	na[e]	727	204
1 min	499	99	na[e]	na[e]	729	216
2.5 min	507	98	592	71	735	194
5 min	520	95	585	90	751	197
10 min	525	118	591	99	>785	na[e]
15 min	529	124	593	99	>785	na[e]
30 min	530	139	598	92	>785	na[e]
45 min	528	158	599	91	>785	na[e]
			270 °C Injection			
30 s	485	120	na[e]	na[e]	699	195
1 min	484	131	na[e]	na[e]	691	200
1 min	484	131	na[e]	na[e]	691	200
2.5 min	495	128	578	70	726	199
5 min	506	126	589	72	747	191
10 min	511	151	615	92	765	175
15 min	521	146	605	94	>785	na[e]
30 min	529	144	607	92	>785	na[e]
45 min	532	144	606	86	>785	na[e]
			280 °C Injection			
30 s	489	125	na[e]	na[e]	734	205
1 min	500	116	596	70	736	188
2.5 min	513	113	613	89	759	189
5 min	527	122	613	75	772	163
10 min	546	123	620	65	>785	na[e]
15 min	552	120	623	63	>785	na[e]
30 min	563	120	635	69	>785	na[e]
45 min	573	136	643	79	>785	na[e]
			290 °C Injection			
30 s	491	138	na[e]	na[e]	685	208
1 min	507	129	na[e]	na[e]	724	193
2.5 min	522	123	596	71	745	191
5 min	527	134	607	69	>785	na[e]
10 min	538	152	624	75	>785	na[e]
15 min	538	169	632	76	>785	na[e]
30 min	553	192	641	72	>785	na[e]
45 min	574	228	661	78	>785	na[e]

[a] Full width at half-maximum (fwhm) calculated from absorption spectra. [b] Band gap emission. [c] FWHM calculated from the emission spectra. [d] Surface state emission. All emission spectra were taken with $\lambda_{ex} = 400$ nm, and the emission was recorded from 415 to 785 nm. [e] Not available.

Effect of Injection and Reaction Temperature on $InP_{(QDs)}$. A series of reactions were run to study the effect of reaction temperature on the quality and size of the $InP_{(QDs)}$ formed, when indium(III) myristate is the indium precursor. Table 2 contains the data obtained from the absorption and emission spectra of aliquots of these reactions conducted entirely at 250, 260, 270, 280, and 290 °C. From the

absorption and emission spectra, it is evident that after 30 s at all temperatures, $InP_{(QDs)}$ have already formed. The lower the reaction temperature, the more blue-shifted the absorption feature, implying that the lower the reaction temperature, the smaller the resulting $InP_{(QDs)}$. Over time, the absorption feature red shifts at the various temperatures. At temperatures greater than 270 °C, the absorption feature becomes broad and featureless, implying a dramatic increase in the size distribution. However, at temperatures below 260 °C, the absorption feature remains sharp throughout the entire 45 min. Each reaction was followed for a total of 2 h and exhibited a sharp absorption feature throughout the entire reaction.

The important thing to note is that, regardless of reaction temperature, a sharp absorption feature is apparent for at least a brief period of time. Typically, when relatively monodispersed crops of nanocrystals are being synthesized, a rapid injection of the group V or group VI precursor is required to generate a rapid crop of reactive nuclei. Then typically, the reaction temperature is decreased to a "growth temperature" until the reaction is stopped. Since with $InP_{(QDs)}$ the typical injection temperature is 290−300 °C, our first reactions were conducted at these temperatures; however, we were initially having problems being able to control the rate of reaction and, subsequently, the quality of the final products. We did find that by utilizing a rapid injection at the elevated temperature, followed by a swift decrease in the reaction temperature (by addition of a reaction equivalent of ODE), we had a much better control of the final $InP_{(QDs)}$ quality. This study shows that a decrease in the injection temperature can lead to more precise control in producing high-quality $InP_{(QDs)}$. We also spent a considerable amount of time trying to determine the effect of temperature on the crystallinity of $InP_{(QDs)}$. XRD seems to be the best method of determining the crystallinity of $InP_{(QDs)}$ formed. We have discovered from our reactions that, regardless of the injection temperature (250−300 °C) and time (1−2 h), we consistently find XRD spectra of the same quality as that shown in Figure 4.

Effect of Carboxylate Size on $InP_{(QDs)}$. A series of reactions were conducted to study the effect of carboxylate size on the reaction as a function of time. Table 3 shows the data obtained from the absorption and emission spectra of aliquots of $InP_{(QDs)}$ prepared at 260 and 290 °C from the corresponding indium(III) carboxylate. These reactions were all carried out under the exact same conditions and concentrations, and monitored for 2 h. Only the data for the first 15 min are given in Table 3. An example of the absorption spectral monitoring of an entire reaction conducted at 260 and 290 °C for an indium(III) laurate is shown in Figure 9.

When the reaction temperature is 260 °C, a sharp absorption feature is prominent for up to 45 min. At or slightly after this time, the absorption broadens. When the reaction temperature is 290 °C, this broadening occurs faster, for indium(III) laurate, at or slightly after 15 min. This broadening is a result of "defocusing of size", resulting in a loss of control over the monodispersity. As the reaction progresses, once all the $InP_{(nuclei)}$ are used up, the individual $InP_{(QDs)}$ begin to react to form larger particles, thereby yielding particles with uncontrolled size. For these reasons, only the spectra of aliquots up to 15 min are presented in Table 3. Evolution of the PL spectra with a change in the carboxylate size and growth temperature, for a given reaction, mirrors the evolution of the absorption spectra. A significant broadening of the sharp PL feature, associated with band edge recombination, is observed when the size distribution can no longer be controlled.

Table 3. Effect of Carboxylate Size on Absorption and Emission Spectra of $InP_{(QDs)}$ at Injection Temperatures of 260 and 290 °C

time	λ_{max} (nm)	FWHM[a] (nm)	λ_{em-max}[b] (nm)	FWHM[c] (nm)	λ_{em-max}[d] (nm)	FWHM[c] (nm)
Indium(III) Laurate Inject at 260 °C						
30 s	511	74	na[e]	na[e]	741	119
1 min	518	74	na[e]	na[e]	770	163
2.5 min	521	76	na	na[e]	774	162
5 min	525	76	na[e]	na[e]	780	159
10 min	527	86	na[e]	na[e]	785	170
15 min	526	86	na[e]	na[e]	785	170
Indium(III) Myristate Inject at 260 °C						
30 s	488	106	na[e]	na[e]	727	204
1 min	499	99	na[e]	na[e]	729	216
2.5 min	507	98	592	71	735	194
5 min	520	95	585	90	751	197
10 min	525	118	591	99	>785	na[e]
15 min	529	124	593	99	>785	na[e]
Indium(III) Stearate Inject at 260 °C						
30 s	464	94	513	59	603	na[e]
1 min	456	102	526	59	607	na[e]
2.5 min	487	80	538	63	635	na[e]
5 min	496	85	550	64	na[e]	na[e]
10 min	496	105	556	81	na[e]	na[e]
15 min	504	101	566	83	na[e]	na[e]
Indium(III) Laurate Inject at 290 °C						
30 s	525	109	na[e]	na[e]	>785	na[e]
1 min	538	94	na[e]	na[e]	>785	na[e]
2.5 min	550	87	na[e]	na[e]	>785	na[e]
5 min	560	86	na[e]	na[e]	>785	na[e]
10 min	561	93	na[e]	na[e]	>785	na[e]
15 min	565	93	630	59	>785	na[e]
Indium(III) Myristate Inject at 290 °C						
30 s	491	138	na[e]	na[e]	685	208
1 min	507	129	na[e]	na[e]	724	193
2.5 min	522	123	596	71	745	191
5 min	527	134	607	69	>785	na[e]
10 min	538	152	624	75	>785	na[e]
15 min	538	169	632	76	>785	na[e]
Indium(III) Stearate Inject at 290 °C						
30 s	485	99	548	75	642	na[e]
1 min	495	90	557	74	669	na[e]
2.5 min	502	109	568	76	696	na[e]
5 min	530	78	579	89	706	na[e]
10 min	483	160	585	94	722	na[e]
15 min	510	133	585	91	725	na

[a] Full width at half-maximum (fwhm) calculated from absorption spectra. [b] Band gap emission. [c] FWHM calculated from the emission spectra. [d] Surface state emission. All emission spectra were taken with $\lambda_{ex} = 400$ nm, and the emission was recorded from 415 to 785 nm. [e] Not available.

We believe that regardless of the size of the carboxylate chain length, high-quality $InP_{(QDs)}$ can be prepared. The difference in the various reactions is the size of the $InP_{(QDs)}$ that are obtained, which can be correlated to the wavelength of the absorbance feature. The size distribution is not dramatically affected by the size of the carboxylate chain length, as determined by the width of the absorption feature. These reactions in which the injection temperature was maintained throughout the course of the reaction do not produce high-quality $InP_{(QDs)}$. However, with this information, high-quality $InP_{(QDs)}$ that emit throughout the majority of the visible

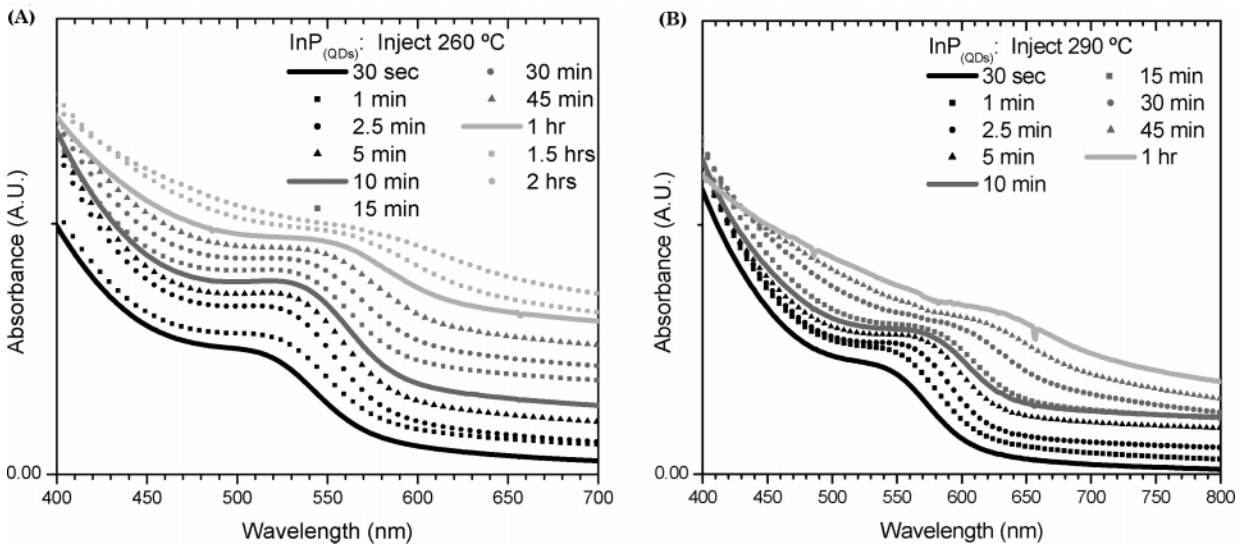

Figure 9. Indium(III) laurate reacted with $P(TMS)_3$ at 260 (A) and 290 °C (B).

spectrum can easily be prepared. For example, if one desired high-quality $InP_{(QDs)}$ that emit at ~520 nm then by simply looking at Table 3, you would know to use indium(III) stearate as your indium precursor and inject at 260 °C, then add a reaction equivalent of ODE after ~30 s, set reaction temperature to 180 °C, and allow the reaction to proceed for a total of 2 h. To obtain high-quality $InP_{(QDs)}$ that emit at 630 nm, use indium(III) laurate as your precursor, inject at 290 °C and add ODE after 15 min, set the growth temperature to 180 °C, and allow the reaction to proceed for a total of 2 h. We define high-quality $InP_{(QDs)}$ as particles with the properties shown in the first part of this text. They are relatively monodispersed with moderate luminescence and highly crystalline with no impurities. Their luminescence efficiency can be dramatically enhanced by quenching surface state recombination through HF etching or covering the surface with a wider band gap semiconductor material. Thus, using this synthetic method, relatively monodispersed crops of high-quality $InP_{(QDs)}$ can be easily prepared, with a variable absorption band covering a major portion of the visible spectrum.

Conclusions and Future Work

The synthesis of high-quality $InP_{(QDs)}$ has been accomplished without the need of an added coordinating ligand or surfactant. Using this fast and reproducible synthesis, $InP_{(QDs)}$ that emit throughout most of the visible spectrum can be obtained. This is the first example of the synthesis of relatively monodispersed crops of $InP_{(QDs)}$ without the addition of any surfactants or coordinating ligands.[39] After an HF etching process, highly luminescent $InP_{(QDs)}$ are obtained.

We are currently extending this methodology to the synthesis of all II−VI and III−V quantum dots, as well as to the synthesis of core−shell and multiple layered semiconductor nanoassemblies (i.e., core−buffer−shell).

Acknowledgment. We acknowledge and thank Rich Nowak for the collection and help in the interpretation of the XPS data. We also thank Liping Guo for doing the TEM and ED imaging, Dave Bordan for collecting the XRD data, and Peter Bush for collecting the EDAX data. This work is supported by the Directorate of Chemistry and Life Sciences of Air Force Office Research through DURINT Grant AFOSR 1016565-1-21169.

Supporting Information Available: Photoluminescence emission and excitation spectra of $InP_{(QDs)}$ (Figure S1), energy dispersive X-ray spectrum of pyridine-washed $InP_{(QDs)}$ (Figure S2), effect of reaction temperature on the absorption spectra of $InP_{(QDs)}$ (Figure S3), effect of reaction temperature on the emission spectra of $InP_{(QDs)}$ (Figure S4), effect of carboxylate ligand size on the absorption spectra of $InP_{(QDs)}$ prepared at 260 and 290 °C, respectively (Figure S5), and effect of carboxylate ligand size on the emission spectra of $InP_{(QDs)}$ prepared at 260 and 290 °C, respectively (Figure S6) (PDF). This material is available free of charge via the Internet at http://pubs.acs.org.

CM050110A

(39) To help clarify, in response to a reviewer's question, Battaglia and Peng[27] have demonstrated the preparation of $InP_{(QDs)}$ utilizing a new method in ODE. In this work,[27] indium(III) acetate and a fatty acid (long chain carboxylic acid) are placed into a reaction vessel and ODE is added. At some point, all of the precursors become soluble and some new species or multiple new species are formed. Then to this mixture of indium carboxylate−acetate species, is added a phosphine or arsine precursor to prepare $InP_{(QDs)}$ or $InAs_{(QDs)}$, respectively. In Bataglia and Peng's short communication, no work or effort was put forth to prove what the reactive indium species was, and we do not feel that it is our place to discuss what intermediates may have been formed under their reaction conditions. The important message in this article is that pure indium(III) carboxylates are prepared separately and characterized before being treated with pure $P(TMS)_3$ to yield high-quality $InP_{(QDs)}$. Our method is the first example in which one pure indium species is weighed out and placed directly into the reaction vessel whereby that pure species is dissolved in unreactive ODE and treated with a phosphine source. To the best of our knowledge, no other reaction conditions have been able to accomplish this in noncoordinating solvents yielding high-quality $InP_{(QDs)}$.